Journal of Engineering Mathematics **27**: 343–356, 1993.

Slip flow in converging and diverging channels

J.M. DORREPAAL
Department of Mathematics & Statistics, Old Dominion University, Norfolk, VA 23529, U.S.A.

Received 27 August 1992; accepted in revised form 14 January 1993

Abstract. The classical problem of Jeffery-Hamel flow is considered in which the fluid is allowed to slip along the walls of the channel. The problem is solved analytically and the volumetric flow rate is computed and compared with that of the corresponding no-slip flow. In the converging channel case, it is found that the slip boundary condition enhances flow rates through the channel, although the effect is minimal when the Reynolds number is large.

In the case of the diverging channel, the slip boundary condition in some instances actually lowers the flow rate from its no-slip value. In other instances, a stable velocity profile does not even appear to exist. These cases aside, when the mean pressure in the channel is adverse, slip flow solutions exist and increase the flow rate through the channel by at most 15.7%.

1. Introduction

The flow of a viscous incompressible fluid in a converging or diverging channel is one of the few exact solutions of the Navier-Stokes equations which is known analytically. The problem has been treated by a number of authors including Goldstein [1], Fraenkel [2], Rosenhead [3] and Batchelor [4] who have shown that the flow characteristics in the two channels are very different. In the converging channel, the flow exhibits boundary layers along each wall while in the diverging channel, the flow can actually change direction at the walls if the Reynolds number is sufficiently large.

More recently, Hooper et al. [5] have shown that the velocity profile can change discontinuously as the Reynolds number R is increased. At critical values of R, the solution jumps from one branch curve in parameter space to another. This jump is accompanied by a very large increase in the wall pressure gradient. In another paper, Sobey and Drazin [6] examine the stability of these Jeffery-Hamel flows. They conclude that flows exhibiting pure outflow or pure inflow are stable. When separation occurs, however, the flow becomes unstable to an antisymmetric mode. In this paper we will restrict our attention to stable Jeffery-Hamel solutions.

The above flows are normally solved subject to the no-slip condition at the channel walls. However, another boundary condition which has commanded interest in certain hydrodynamical contexts is the slip condition. In this condition the fluid velocity at a rigid boundary is proportional to the shear stress. The fluid slips along the boundary and the retarding influence of the boundary on the flow is modified.

A number of authors have considered the effects of the slip boundary condition. In his book, Lamb [7] records how the slip condition modifies the drag experienced by a sphere in Stokes flow. Tsien [8] considers slip flow in a pipe and shows that the velocity distribution across a section of the pipe is more uniform than in the no-slip case. Laurmann [9] uses the Oseen equations to consider slip flow past a semi-infinite flat plate and later, Van de Vorren and Veldman [10] show that the slip condition modifies the singularity in the shear stress at the leading edge of the plate. Tamada and Miura [11] treat the slip flow past a finite flat plate

which is aligned with the flow and Miura [12] subsequently considers the case when the plate is inclined to the flow.

In this paper we consider slip flow in both converging and diverging channels. We are motivated by the fact that these problems provide rare examples where slip flow solutions of the Navier-Stokes equations can be treated analytically. The problems also serve to model channel flows where a thin lubricant layer lines the walls thus suggesting the slip condition. In this context it is interesting to compare the volumetric flux through the channel when the slip condition is in effect with the flux corresponding to the no-slip flow. It will be our purpose to calculate this flux ratio whenever a slip flow solution is found.

The classical no-slip solutions given by Fraenkel [2] are presented in section 2 for reference. In section 3, the problem of slip flow in a converging channel is solved and in section 4, the diverging channel case is analyzed. The results of our investigation are summarized in section 5.

2. No-slip Jeffery-Hamel flow

Following Fraenkel [2], we adopt the following notation (Fig. 1). Let (r, θ) be polar coordinates; $u(r, \theta)$ the radial component of velocity; α the semi-angle of the wedge-shaped channel; and let ν and ρ be the kinematic viscosity and fluid density respectively.

We take as known physical parameters the angle $\alpha > 0$ and a Reynolds number R based on the volumetric flow rate through the channel:

$$M = \frac{1}{2}\int_{-\alpha}^{\alpha} ru \, d\theta \,, \quad R = \frac{M}{\nu} \,. \tag{2.1}$$

Negative values of R correspond to flows in a converging channel and positive values of R indicate flows in a diverging channel. We take $y = \theta/\alpha$ as independent variable, and define a non-dimensional velocity function

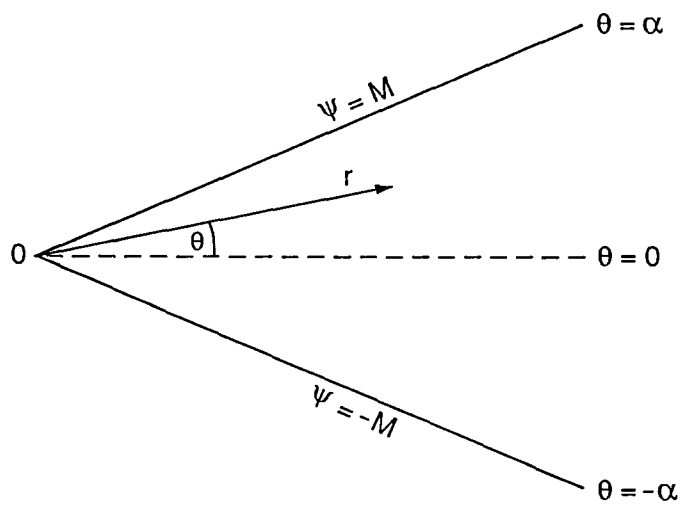

Fig. 1. Notation

$$g(y) = \frac{\alpha r u(r, y)}{M} . \tag{2.2}$$

Since we are considering only cases of pure inflow or pure outflow, we assume the velocity is symmetric about the channel center-line. With the notation of (2.1) and (2.2), the differential equation for the velocity function is

$$g''(y) + 4\alpha^2 g(y) + \alpha \mathrm{R} g(y)^2 = -A , \tag{2.3}$$

where A is a constant proportional to the wall pressure gradient. The boundary conditions are as follows:

(i) no-slip condition: $g(1) = 0 ,$ (2.4a)

(ii) symmetry condition: $g'(0) = 0 ,$ (2.4b)

(iii) flux condition: $\int_0^1 g(y)\, dy = 1 .$ (2.4c)

Once the velocity is determined, the pressure can be obtained from the relation

$$p(r, y) - p_\infty = \frac{\rho \mathrm{R} \nu^2}{2\alpha^3 r^2} [A + 4\alpha^2 g(y)] . \tag{2.5}$$

In the case of inflow ($\mathrm{R} < 0$), Fraenkel [2] has shown that the velocity function is given explicitly by

$$g(y) = \frac{2}{\alpha \mathrm{R}} \{b^2(1 + m) - \alpha^2 - 3mb^2 \operatorname{cd}^2(by, m)\} , \tag{2.6}$$

where (b, m) are modified constants of integration and $\operatorname{cd}(by, m)$ is a Jacobi elliptic function with modulus $k = m^{1/2}$.

The relationship between constants (b, m) and parameters (R, α) is obtained by invoking conditions (2.4a) and (2.4c). We therefore obtain

$$b^2(1 + m) - \alpha^2 - 3mb^2 \operatorname{cd}^2(b, m) = 0 , \tag{2.7a}$$

$$b^2(1 + m) - \alpha^2 - 3b[b - E_*(b, m)] - 3mb \operatorname{sn}(b, m) \operatorname{cd}(b, m) = \frac{1}{2} \alpha \mathrm{R} , \tag{2.7b}$$

where $\operatorname{sn}(b, m)$ is another elliptic function and $E_*(b, m)$ is the elliptic integral of the second kind. Values of (b, m) corresponding to specific points (R, α) in parameter space can be obtained using a two-dimensional Newton's method on the system of equations in (2.7). Fraenkel labels solutions of the form given in (2.6) as Type III solutions.

In the case of outflow ($\mathrm{R} > 0$), the solution to (2.3) has two forms depending on whether a certain cubic has complex roots or not. The Type I solution has the form

$$g(y) = \frac{2}{\alpha \mathrm{R}} \{2a^2(2m - 1) - \alpha^2 - 3a^2 \operatorname{sn}^2(ay, m) \operatorname{dc}^2(ay, m)\} , \tag{2.8}$$

where dc is the elliptic function inverse to cd. The relationship between constants (a, m) and parameters (R, α) is given by

$$2a^2(2m-1) - \alpha^2 - 3a^2 \operatorname{sn}^2(a,m) \operatorname{dc}^2(a,m) = 0\,, \tag{2.9a}$$

$$2a^2\left(2m - \frac{5}{2}\right) - \alpha^2 + 6aE_*(a,m) - 3a \operatorname{sn}(a,m) \operatorname{dc}(a,m) = \frac{1}{2}\alpha \mathrm{R}\,. \tag{2.9b}$$

The Type II solution has the form

$$g(y) = \frac{2}{\alpha \mathrm{R}} \{b^2(1+m) - \alpha^2 - 3mb^2 \operatorname{sn}^2(by, m)\}\,, \tag{2.10}$$

where

$$b^2(1+m) - \alpha^2 - 3mb^2 \operatorname{sn}^2(b,m) = 0\,, \tag{2.11a}$$

$$b^2(1+m) - \alpha^2 - 3b[b - E_*(b,m)] = \frac{1}{2}\alpha \mathrm{R}\,. \tag{2.11b}$$

A significant insight from Fraenkel's paper is that the three solutions (2.6, 2.8, 2.10) complement each other in parameter space (R, α). The situation is illustrated in Fig. 2. The regions in the plane where the various solutions are valid are indicated by Roman numerals. The boundary curves are denoted by $\mathcal{B}_i, i = -2, -1, 1, 2, 3$. The Type I and Type II solutions are analytic continuations of each other across $\mathcal{B}_1$, whose equation can be obtained

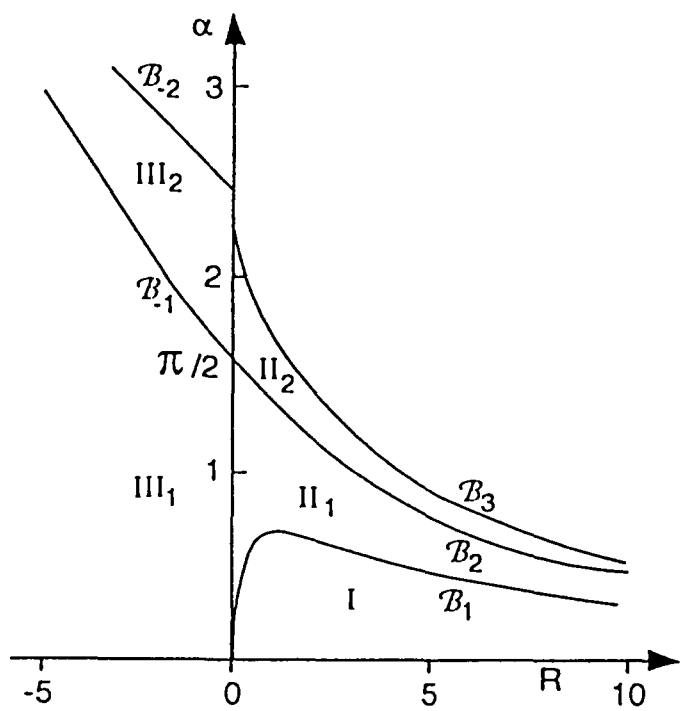

Fig. 2. The (R, α) plane with regions corresponding to Type I, Type II and Type III solutions.

by setting $m = 1$ in either (2.9) or (2.11). Doing so yields the following parametric representation for $\mathscr{B}_1$:

$$\alpha = b(2 - 3\tanh^2 b)^{1/2}\,,$$
$$\mathrm{R} = \frac{6(b\tanh^2 b + \tanh b - b)}{(2 - 3\tanh^2 b)^{1/2}}\,, \tag{2.12}$$

where $0 \leqslant b < 1.1462$.

Region II_1 contains solutions exhibiting pure outflow in a diverging channel. Region II_2 corresponds to diverging flows which exhibit outflow near the center of the channel and inflow along the walls. Sobey and Drazin [6] note that solutions in region II_2 are unstable and that boundary $\mathscr{B}_2$ is a curve of marginal stability. Indeed it is the curve whose points represent solutions having vanishing tangential stress at the channel walls thus making separation and reverse flow imminent. The values of R at points (R, α) along $\mathscr{B}_2$ are critical Reynolds numbers for the corresponding channel angles α. Table 1 provides critical Reynolds numbers R_c for channel angles $15° \leqslant \alpha \leqslant 65°$.

A parametric representation for $\mathscr{B}_2$ is obtained by substituting $b = K(m)$ into (2.11) where $K(m)$ is the complete elliptic integral of the first kind. The resulting equations are

$$\alpha = (1 - 2m)^{1/2} K(m)\,,$$
$$\mathrm{R}_c = \frac{6K(m)}{\alpha}\{E(m) - (1 - m)K(m)\}\,, \tag{2.13}$$

where $0 \leqslant m < \frac{1}{2}$ and $E(m)$ is the complete elliptic integral of the second kind. As $m \to \frac{1}{2}$, we have $\alpha \to 0$ and $\mathrm{R}_c \to +\infty$ such that

$$\alpha \mathrm{R}_c = 6K(\tfrac{1}{2})E(\tfrac{1}{2}) - 3K(\tfrac{1}{2})^2 = \tfrac{3}{2}\pi\,, \tag{2.14}$$

where the simplification to $\frac{3}{2}\pi$ is due to Legendre's Relation [13].

In a similar way, curve $\mathscr{B}_{-1}$ marks the boundary between solutions exhibiting pure inflow in a converging channel (III_1) and those exhibiting reverse flow along the walls of the channel (III_2). The substitution $b = K(m)$ into equations (2.7) gives a parametric representation for $\mathscr{B}_{-1}$. It is clear from Fig. 2 that separation in a converging channel can only occur

Table 1. Critical Reynolds numbers R_c for channels with semi-angle α

α	R_c
15°	17.5246
20°	12.8653
25°	10.0054
30°	8.0447
35°	6.5973
40°	5.4701
45°	4.5560
50°	3.7905
55°	3.1325
60°	2.5546
65°	2.0378

when $\alpha > \frac{1}{2}\pi$ and since all flows considered in this paper are in concave channels, we will not be concerned with details regarding $\mathscr{B}_{-1}$.

The curves $\mathscr{B}_{-2}$ and $\mathscr{B}_3$ are boundaries along which the Jacobian $\partial(\mathrm{R}, \alpha)/\partial(b, m)$ defined by the relations in (2.7) or (2.11) vanishes. Hooper et al. [5] show that as a solution approaches this curve, it experiences a jump to another branch not pictured in Fig. 2 with an accompanying discontinuous change in the velocity profile. According to Sobey and Drazin [6], however, solutions in this region of the (R, α) plane are unstable and we will not consider them further in this paper.

3. Slip flow in a converging channel

Let $f(y)$ be the velocity function for a slip flow in a converging channel with semi-angle α. The boundary value problem for $f(y)$ involves the differential equation in (2.3) and the boundary conditions in (2.4) with the no-slip condition replaced by

$$f(1) + \lambda f'(1) = 0\,, \tag{3.1}$$

where $\lambda > 0$ is the slip coefficient. The parameters in this problem are α and λ. The slip Reynolds number R_s is proportional to the volumetric flux through the channel and is determined by the additional condition that the mean pressure $\bar{p}(r)$ in the slip flow be identical to that of the corresponding no-slip flow. From (2.5) we have

$$\bar{p}(r) = \frac{1}{2}\int_{-1}^{1} p(r, y)\,\mathrm{d}y = p_\infty + \frac{\rho \mathrm{R}\nu^2}{2\alpha^3 r^2}(A + 4\alpha^2)\,. \tag{3.2}$$

If the constants R, A correspond to no-slip flow and R_s, A_s correspond to slip flow, the mean pressure condition becomes

$$\mathrm{R}_s(A_s + 4\alpha^2) = \mathrm{R}(A + 4\alpha^2)\,. \tag{3.3}$$

The velocity function for slip flow in a converging channel has exactly the same form as in the no-slip case. Thus from (2.6), we have

$$f(y) = \frac{2}{\alpha \mathrm{R}_s}\{\tilde{b}^2(1 + \tilde{m}) - \alpha^2 - 3\tilde{m}\tilde{b}^2\,\mathrm{cd}^2(\tilde{b}y, \tilde{m})\}\,, \tag{3.4}$$

where the tildas represent the slip flow constants. The symmetry condition $f'(0) = 0$ is automatically satisfied by (3.4) and so the three constants $\tilde{b}$, $\tilde{m}$, R_s are determined by the slip condition (3.1), the mean pressure condition (3.3) and the flux condition

$$\int_0^1 f(y)\,\mathrm{d}y = 1\,. \tag{3.5}$$

The pressure coefficient A_s in (3.3) can be expressed in terms of $\tilde{b}$, $\tilde{m}$, R_s using the differential equation satisfied by $f(y)$. We have

$$f''(y) + 4\alpha^2 f(y) + \alpha \mathrm{R}_s f(y)^2 = -A_s\,, \tag{3.6}$$

which yields, after some simplification,

$$A_s = \frac{4}{\alpha R_s}\{\alpha^4 - \tilde{b}^4(1 - \tilde{m} + \tilde{m}^2)\}\,. \tag{3.7}$$

In a similar way, the no-slip coefficient A in (3.3) can be expressed in terms of b, m, R using (2.3) and (2.6). When these expressions are substituted into (3.3), the mean pressure condition takes the form

$$\alpha^3 R_s - \tilde{b}^4(1 - \tilde{m} + \tilde{m}^2) = \alpha^3 R - b^4(1 - m + m^2)\,, \tag{3.8}$$

where the right side is known for any given no-slip flow.

Equation (3.8) enables us to express R_s explicitly in terms of $\tilde{b}$ and $\tilde{m}$ with the result that the slip condition (3.1) and the flux condition (3.5) can be given solely in terms of $\tilde{b}$ and $\tilde{m}$. After some tedious calculations, the equations are

$$\tilde{b}^2(1 + \tilde{m}) - \alpha^2 - 3\tilde{m}\tilde{b}^2\,\mathrm{cd}^2(\tilde{b}, \tilde{m}) + 6\lambda\tilde{m}(1 - \tilde{m})\tilde{b}^3\,\mathrm{sn}(\tilde{b}, \tilde{m})\,\mathrm{cn}(\tilde{b}, \tilde{m})/\mathrm{dn}^3(\tilde{b}, \tilde{m}) = 0\,, \tag{3.9a}$$

$$\tilde{b}^2(1 + \tilde{m}) - \alpha^2 - \tilde{b}^4(1 - \tilde{m} + \tilde{m}^2)/2\alpha^2 - 3\tilde{b}[\tilde{b} - E_*(\tilde{b}, \tilde{m})] - 3\tilde{m}\tilde{b}\,\mathrm{sn}(\tilde{b}, \tilde{m})\,\mathrm{cn}(\tilde{b}, \tilde{m})/\mathrm{dn}(\tilde{b}, \tilde{m}) = T\,, \tag{3.9b}$$

where $T = \frac{1}{2}\alpha R - b^4(1 - m + m^2)/2\alpha^2$ is a constant determined from the corresponding no-slip flow. Given α, λ and T, Newton's method is used to determine the values of $\tilde{b}$ and $\tilde{m}$ which in turn are used to evaluate the slip Reynolds number R_s:

$$R_s = 2T/\alpha + \tilde{b}^4(1 - \tilde{m} + \tilde{m}^2)/\alpha^3\,. \tag{3.10}$$

The data in Table 2 illustrates a typical relationship between flux ratio R_s/R and slip coefficient λ. The flows occur in a channel having semi-angle 65° and the no-slip Reynolds number is $R = -1$. When $\lambda = 0$, we recover the no-slip case and the flux ratio is unity. As λ increases from zero, the flux ratio grows dramatically at first and then appears to approach a limit as $\lambda \to +\infty$. The limit can be calculated by recognizing that as $\lambda \to +\infty$, we have $\tilde{m} \to 0$ in such a way that $\lambda\tilde{m} \to$ constant. If the limit $\tilde{m} \to 0$ is taken in equations (3.9b) and (3.10), we can eliminate $\tilde{b}$ from the resulting two equations to get

$$\lim_{\lambda \to +\infty} \frac{R_s}{R} = -\frac{2}{R}(-2T - \alpha^2)^{1/2}\,. \tag{3.11}$$

Table 2. Flux ratio R_s/R vs slip coefficient λ for slip flows in a converging channel with $\alpha = 65°$, $R = -1$.

λ	$\tilde{b}$	$\tilde{m}$	R_s/R
0.0	1.1272	0.3458	1.0000
0.3	1.0298	0.3381	1.2577
1.0	0.8968	0.3118	1.5075
2.0	0.8024	0.2786	1.6287
5.0	0.6881	0.2133	1.7277
10.0	0.6217	0.1555	1.7666
100.0	0.5260	0.0274	1.8045
1000.0	0.5124	0.0030	1.8084

Table 3. Perfect slip flux ratio ($\lim_{\lambda\to+\infty} R_s/R$) as a function of no-slip Reynolds number R and channel semi-angle α

R	$\alpha = 15°$	$\alpha = 40°$	$\alpha = 65°$
−1.0	3.5761	2.2989	1.8089
−2.0	2.6745	1.8439	1.5544
−5.0	1.9360	1.4886	1.3465
−10.0	1.6072	1.3307	1.2441
−20.0	1.4013	1.2269	1.1715

The limit is well-defined because T is always sufficiently negative to make the right hand expression real. Table 3 gives flux ratio R_s/R versus no-slip Reynolds number R in the perfect slip limit ($\lambda = +\infty$) for three different channel angles $\alpha = 15°, 40°, 65°$.

The data in Table 3 reveal that significant increases in flow rates through a converging channel can be realized when friction along the channel walls is removed. In fact, in the perfect slip limit the velocity profile is precisely uniform with velocity function $f(y) \equiv 1$. The flux ratios in Table 3 diminish as $|R|$ gets large because the no-slip profiles for large $|R|$ are almost uniform across most of the channel with very thin boundary layers along each wall. Thus as $|R|$ gets large, the no-slip and perfect slip velocity profiles are very similar and the flux ratio approaches unity. This can be seen as follows.

Equation (3.11) can be written in the equivalent form

$$\lim_{\lambda\to+\infty} \frac{R_s}{R} = \left(-\frac{2}{\alpha R}\right)[b^4(1-m+m^2) - \alpha^3 R - \alpha^4]^{1/2}, \tag{3.12}$$

where (b, m) are related to (R, α) through equations (2.7ab). Computations involving (2.7ab) reveal that as $R\to-\infty$ with α fixed, we have $m\to 1$ and $b\to+\infty$. Thus from (2.7a), we have $\mathrm{cd}(b, m)\to(\frac{2}{3})^{1/2}$. Because $\mathrm{sn}(b, m)$ and $E_*(b, m)$ are $O(1)$, the dominant terms on the left side of (2.7b) are the terms of $O(b^2)$. Thus from (2.7b), we have

$$b \sim (-\tfrac{1}{2}\alpha R)^{1/2}. \tag{3.13}$$

When this is substituted into (3.12), we obtain the aforementioned result

$$\lim_{R\to-\infty}\left(\lim_{\lambda\to+\infty}\frac{R_s}{R}\right) = 1. \tag{3.14}$$

4. Slip flow in a diverging channel

The formulation of the problem in a diverging channel is complicated by the fact that diverging channel flows can be described by Type I solutions or Type II solutions. It is found, however, that when the slip coefficient λ is positive, the curve $\mathscr{B}_1$ in (R, α) parameter space retains the same general shape as in the no-slip case but is uniformly closer to the R-axis (see Fig. 2). Thus in comparing a slip flow with its no-slip counterpart, we may have (i) a Type II slip flow matched up with a Type II no-slip flow; (ii) a Type II slip flow matched up with a Type I no-slip flow; or (iii) a Type I slip flow matched up with a Type I no-slip flow. In the interests of brevity, we will formulate case (i) and comment on the other possibilities only when they arise.

With this clarification, the formulation of the diverging channel case is similar to the converging channel problem outlined in section 3. The velocity function has the form given in (2.10), namely

$$f(y) = \frac{2}{\alpha \mathrm{R}_s} \{\tilde{b}^2(1+\tilde{m}) - \alpha^2 - 3\tilde{m}\tilde{b}^2 \,\mathrm{sn}^2(\tilde{b}y, \tilde{m})\}\,, \tag{4.1}$$

and the boundary conditions necessary to determine $\tilde{b}$, $\tilde{m}$, R_s are as follows:

(i) slip condition: $$f(1) + \lambda f'(1) = 0\,, \tag{4.2a}$$

(ii) flux condition: $$\int_0^1 f(y)\,\mathrm{d}y = 1\,, \tag{4.2b}$$

(iii) pressure condition: $$\bar{p}_s(r) = \bar{p}(r)\,, \tag{4.2c}$$

where $\bar{p}_s(r)$ is the mean pressure associated with the slip flow and $\bar{p}(r)$ is the mean pressure for the corresponding no-slip flow. The calculation of the mean pressures from the respective velocity functions is routine and it is found that the pressure condition in the diverging channel problem has exactly the same form as in the converging channel case:

$$\alpha^3 \mathrm{R}_s - \tilde{b}^4(1 - \tilde{m} + \tilde{m}^2) = \alpha^3 \mathrm{R} - b^4(1 - m + m^2) = 2\alpha^2 T\,, \tag{4.3}$$

where T is defined in the same way as in section 3. By solving (4.3) for R_s, we can eliminate R_s from the flux condition (4.2b) and thus obtain two equations for the slip flow constants $\tilde{b}$ and $\tilde{m}$:

$$\tilde{b}^2(1+\tilde{m}) - \alpha^2 - 3\tilde{m}\tilde{b}^2 \,\mathrm{sn}^2(\tilde{b}, \tilde{m}) - 6\lambda\tilde{m}\tilde{b}^3 \,\mathrm{sn}(\tilde{b}, \tilde{m})\,\mathrm{cn}(\tilde{b}, \tilde{m})\,\mathrm{dn}(\tilde{b}, \tilde{m}) = 0\,, \tag{4.4a}$$

$$\tilde{b}^2(1+\tilde{m}) - \alpha^2 - \tilde{b}^4(1 - \tilde{m} + \tilde{m}^2)/2\alpha^2 - 3\tilde{b}[\tilde{b} - E_*(\tilde{b}, \tilde{m})] = T\,. \tag{4.4b}$$

The procedure then is as follows. For given values of α and R, the no-slip flow in a diverging channel is found. The value of T is calculated for this particular flow. The slip coefficient λ is assigned a value and the three constants α, λ, T are substituted into (4.4). Using Newton's method, the corresponding values of $\tilde{b}$ and $\tilde{m}$ are determined and then used to calculate R_s in (4.3). The flux ratio R_s/R measures how much more efficiently the slip flow transports fluid through the channel.

The diverging channel flows differ from the converging flows in section 3 in that the no-slip diverging flows separate and become unstable at the critical Reynolds number R_c. Since we are considering only stable flows in this paper, the no-slip Reynolds number has a finite range: $0 \leqslant \mathrm{R} \leqslant \mathrm{R}_c$. It was mentioned in section 2 that when $\mathrm{R} = \mathrm{R}_c$, the tangential stress vanishes along the wall. Thus when $\mathrm{R} = \mathrm{R}_c$, the velocity function $g(y)$ given by (2.10) satisfies $g(1) = 0$ by virtue of the no-slip condition and also $g'(1) = 0$ by virtue of the vanishing tangential stress. The end result is that even though $g(y)$ is a no-slip velocity profile, it satisfies the slip boundary condition (4.2a) for *all* $\lambda \geqslant 0$. In fact, when $\mathrm{R} = \mathrm{R}_c$, the no-slip velocity function $g(y)$ satisfies all boundary conditions in (4.2). At the critical Reynolds number, therefore, the slip flow in a diverging channel is identical to the no-slip flow and the flux ratio R_s/R is unity.

When $\mathrm{R} < \mathrm{R}_c$, slip flow in a diverging channel is much more complicated than slip flow in

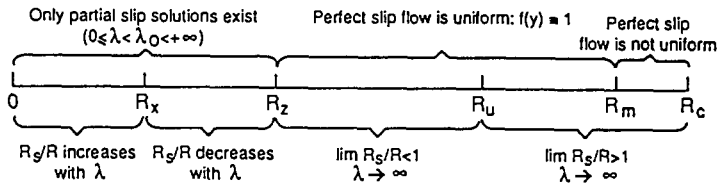

Fig. 3. Slip flow regimes as subintervals of $[0, R_c]$.

a converging channel. In fact, as R increases through the interval $[0, R_c]$, there are five different regimes through which the slip flows pass. In Fig. 3 these regimes are depicted as subintervals of $[0, R_c]$. The endpoints of these subintervals R_x, R_z, R_u, R_m are no-slip Reynolds numbers which act as transition points from one slip flow regime into another. The five-regime structure is present for all channel angles $0 < \alpha < \frac{1}{2}\pi$.

Regime I: [0, R_x]

When $0 < R < R_x$, it is found that the system of equations in (4.4) does not have a solution for all $\lambda > 0$. In particular, taking $F(\tilde{b}, \tilde{m}, \lambda)$ and $G(\tilde{b}, \tilde{m})$ as the left sides of (4.4a) and (4.4b) respectively, it can be shown that the Jacobian $\partial(F, G)/\partial(\tilde{b}, \tilde{m})$ vanishes at a finite value λ_0. Slip flow solutions only exist therefore for $0 \leq \lambda < \lambda_0$. Typical values of λ_0 seem to be quite small and depend on both α and R, although exhaustive tables were not calculated. We did find that for $\alpha = 65°$ and $R = \frac{1}{6}R_c = 0.3396$, the value of λ_0 was in the range $0.014 < \lambda_0 < 0.015$. For $\alpha = 40°$ and $R = \frac{1}{6}R_c = 0.9117$, we found $0.008 < \lambda_0 < 0.009$.

As λ increases from 0 to λ_0, the flux ratio R_s/R increases. Table 4 contains results for a couple of cases.

When $R = R_x$, the Jacobian $\partial(F, G)/\partial(\tilde{b}, \tilde{m})$ corresponding to (4.4) vanishes at $\lambda = 0$. This means that slip flows of the form (4.1) are not possible for any $\lambda > 0$ at this Reynolds number. This surprising result will be discussed further in section 5. It should be added, however, that even though the Jacobian vanishes at $\lambda = 0$, the system of equations for $\lambda = 0$ has the solution $\tilde{b} = b$, $\tilde{m} = m$ where b and m are defined by (2.11). Therefore the no-slip solution can be recovered from (4.4) even though no solution exists for $\lambda > 0$.

Regime II: [R_x, R_z]

When $R_x < R < R_z$, the system of equations in (4.4) again has a solution for λ in the range $0 \leq \lambda < \lambda_0$. As before typical values of λ_0 are small and include $\lambda_0 \approx 0.24$ when $\alpha = 40°$, $R = \frac{1}{3}R_c = 1.8234$ and $\lambda_0 \approx 0.33$ when $\alpha = 65°$, $R = \frac{1}{3}R_c = 0.6793$. The difference in this regime is that as λ increases from 0 to λ_0, the flux ratio R_s/R decreases. Thus the flow rate in

Table 4. Flux ratios for various channel angles α and slip coefficients λ with $R = \frac{1}{6}R_c$.

λ	$\alpha = 40°$	$\alpha = 65°$
0.0	1.0000	1.0000
0.001	1.0112	1.0067
0.005	1.0674	1.0363
0.008	1.1521	1.0630
0.010	——	1.0844
0.014	——	1.1503

Table 5. Flux ratios for various channel angles α and slip coefficients λ with $R = \frac{1}{3}R_c$.

λ	$\alpha = 40°$	$\alpha = 65°$
0.0	1.0000	1.0000
0.05	0.9257	0.9552
0.10	0.8454	0.9068
0.20	0.6477	0.7965
0.23	0.5429	0.7580
0.30	———	0.6440
0.325	———	0.5737

the slip case is actually less than the flow rate in the no-slip case – a paradox which will be discussed further in the next section. Table 5 contains results for the two cases mentioned above.

As R approaches R_z, the value of λ_0 increases dramatically and when $R = R_z$, the range of λ becomes infinite. Therefore R_z is the Reynolds number at which perfect slip flow in a diverging channel is first possible.

Regime III: $[R_z, R_u]$

In this regime the system of equations in (4.4) has a solution for all $\lambda \geqslant 0$. In the perfect slip limit ($\lambda = +\infty$), we have $\tilde{m} = 0$ and the velocity profile is uniform: $f(y) \equiv 1$. The flux ratio R_s/R may grow slightly at first as λ increases from 0, but as λ gets larger the flux ratio behaves like in regime II and decreases. The perfect slip flux ratio ranges from 0 when $R = R_z$ to 1 when $R = R_u$. The zero value for the flux ratio at $R = R_z$ corresponds to the case when the mean pressure in the channel is constant and the fluid is stagnant: $f(y) \equiv 0$.

Regime IV: $[R_u, R_m]$

Like regime III, equations (4.4) have solutions for all $\lambda \geqslant 0$. Unlike regime III, however, the flux ratio is an increasing function of λ. In the perfect slip limit ($\lambda = +\infty$), it ranges from a value of 1 when $R = R_u$ to a maximum value at $R = R_m$ of about 1.157 irrespective of channel angle α.

Regime V: $[R_m, R_c]$

Regime V is a transition regime between slip flows at $R = R_m$ whose velocity profiles become increasingly uniform as λ gets large, and slip flows at $R = R_c$ whose velocity profiles do not change at all as λ increases. When $R_m < R < R_c$, it is found that as $\lambda \to +\infty$ in equations (4.4), we no longer have $\tilde{m} \to 0$. Instead we have $\mathrm{cn}(\tilde{b}, \tilde{m}) \to 0$ which means $\tilde{b} \to K(\tilde{m})$. Thus the perfect slip velocity profile in this regime is no longer uniform, but instead has the form

$$f(y) = \frac{2}{\alpha R_s}\{K(\tilde{m})^2(1+\tilde{m}) - \alpha^2 - 3\tilde{m}K(\tilde{m})^2\,\mathrm{sn}^2[K(\tilde{m})y, \tilde{m}]\}\,, \tag{4.5}$$

obtained from (4.1) by substituting $\tilde{b} = K(\tilde{m})$. The value of $\tilde{m}$ is obtained from (4.4b) by solving

$$K(\tilde{m})^2(1+\tilde{m}) - \alpha^2 - K(\tilde{m})^4(1-\tilde{m}+\tilde{m}^2)/2\alpha^2 - 3K(\tilde{m})[K(\tilde{m}) - E(\tilde{m})] = T\,. \tag{4.6}$$

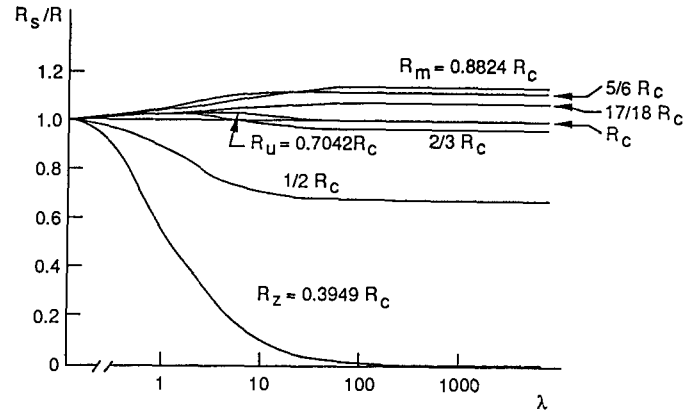

Fig. 4. Flux ratio R_s/R vs. slip coefficient λ for various Reynolds numbers in a diverging channel with semi-angle $\alpha = 65°$.

Table 6. Key Reynolds number ratios for diverging channels with semi-angles $\alpha = 65°$, 40°, 15°.

	$\alpha = 65°$	$\alpha = 40°$	$\alpha = 15°$
R_x/R_c	0.2012	0.1987	0.1968
R_z/R_c	0.3949	0.3890	0.3855
R_u/R_c	0.7042	0.7279	0.7400
R_m/R_c	0.8824	0.8959	0.9033
R_s/R_m	1.1573	1.1574	1.1577

It is found that as R runs from R_m to R_c, the value of $\tilde{m}$ ranges from 0 to m where m is the no-slip value defined in (2.13). The perfect slip flux ratio R_s/R ranges from its maximum value at R_m to the value 1 at $R = R_c$.

Figure 4 is a plot of flux ratio R_s/R versus slip coefficient λ for a variety of Reynolds numbers R in a diverging channel with semi-angle 65°. The values of R are all normalized with respect to the critical Reynolds number for this channel, $R_c = 2.0378$. The transition Reynolds numbers introduced in Fig. 3 are normalized in the same way and the normalized values are given in Table 6. We have also included in Table 6 the normalized values of the transition Reynolds numbers for diverging channels with semi-angles 40° and 15°. The Reynolds numbers corresponding to $\alpha = 40°$ have been scaled by the appropriate critical Reynolds number $R_c = 5.4701$ and the $\alpha = 15°$ values have been scaled by $R_c = 17.5246$.

The data in Table 6 shows that when Reynolds numbers are normalized by the critical value R_c, the transition Reynolds numbers illustrated in Fig. 3 have approximately the same value regardless of channel angle α. In addition, the last row of Table 6 shows that the maximum perfect slip flux ratio R_s/R_m is essentially the same for all channel angles α.

5. Discussion

We conclude the paper by attempting to shed some light on the paradoxical results encountered in the previous section. Their explanation is facilitated by an examination of the mean pressure in the channel.

The mean pressure is computed in (3.2) and for a diverging channel it is easily shown that

$$\mathrm{R}(A + 4\alpha^2) = 8\alpha(T + \tfrac{1}{2}\alpha^2)\,, \tag{5.1}$$

where T is defined in (3.9b). It follows from (3.2) that the mean pressure in a diverging channel depends on radial coordinate r in the following way:

$$\bar{p}(r) - p_\infty \propto (T + \tfrac{1}{2}\alpha^2) r^{-2}\,. \tag{5.2}$$

For Reynolds numbers in the range $0 < \mathrm{R} < \mathrm{R}_z$, the expression $T + \frac{1}{2}\alpha^2$ is positive. Thus the mean pressure decreases as r increases and the pressure gradient is favourable. From Fig. 3, these are precisely the values of R for which only partial slip solutions exist. When $\mathrm{R} = \mathrm{R}_z$, the expression $T + \frac{1}{2}\alpha^2$ vanishes and for $\mathrm{R} > \mathrm{R}_z$, we have $T + \frac{1}{2}\alpha^2 < 0$. It is observed, therefore, that as soon as the pressure gradient in the channel becomes adverse, perfect slip solutions become possible.

It is interesting to speculate on the flow if the Reynolds number R is less than R_z and the slip coefficient is increased through the value λ_0. The fact that the Jacobian of (4.4) vanishes when $\lambda = \lambda_0$ is reminiscent of the Jacobian of (2.11) vanishing when the point (R, α) crosses curve $\mathscr{B}_3$ in Fig. 2. Following the analysis of Hooper, Duffy and Moffatt [5], it is conceivable that at the value λ_0, the slip flow jumps to another branch of solutions whose velocity profiles have regions of inflow as well as outflow. According to the work of Sobey and Drazin [6], such slip flows are unstable. Our conjecture, then, is that when the pressure gradient is favourable $(0 < \mathrm{R} < \mathrm{R}_z)$, the slip flow is unstable for slip coefficients $\lambda > \lambda_0$. Only when the pressure gradient is adverse is it possible to have stable perfect slip flow in a diverging channel.

The second observation is that mean pressure, when considered as a function of Reynolds number, has a maximum at $\mathrm{R} = \mathrm{R}_x$. The proof is not included here but it can be shown from (5.2) that the partial derivative $\partial\bar{p}(r; \mathrm{R})/\partial\mathrm{R}$ vanishes at the same value of R as does $[\partial(F, G)/\partial(\tilde{b}, \tilde{m})]_{\lambda=0}$ where $F(\tilde{b}, \tilde{m}, \lambda)$ and $G(\tilde{b}, \tilde{m})$ are the left sides of (4.4a) and (4.4b) respectively. Thus when $0 < \mathrm{R} < \mathrm{R}_x$, the expression $T + \frac{1}{2}\alpha^2$ in (5.2) is an increasing function of R and the mean pressure gradient

$$\frac{\partial\bar{p}(r; \mathrm{R})}{\partial r} \propto \frac{-2(T + \frac{1}{2}\alpha^2)}{r^3} \tag{5.3}$$

at each point of the channel increases (in absolute value) with R. It was observed in section 4 that in this regime, an increase in slip coefficient λ leads to an increase in flux ratio R_s/R. Now in regime II $(\mathrm{R}_x < \mathrm{R} < \mathrm{R}_z)$, the absolute value of the mean pressure gradient decreases with R at each point of the channel and this is accompanied by a decrease in the flux ratio as λ grows. We find, therefore, that when the pressure gradient is favourable $(0 < \mathrm{R} < \mathrm{R}_z)$, the response of the flux ratio to increases in λ depends upon whether the pressure gradient is an increasing or decreasing function of R.

The final comment relates to the Reynolds number R_z at which value the mean pressure is constant $(T + \frac{1}{2}\alpha^2 = 0)$. How can it be at this Reynolds number that at large values of λ, the flux ratio is almost zero?

In no-slip flows with $\mathrm{R} = \mathrm{R}_z$, even though the mean pressure gradient is zero, there is still a non-constant pressure distribution in the channel. Along the axis of the channel there is a favourable pressure gradient and along the walls the pressure gradient is adverse. The result

is a kind of jet-like flow concentrated in the middle of the channel which drags the fluid near the walls along with it.

Now the effect of a large slip coefficient is to decrease friction at the walls and thus make the velocity distribution across the channel more uniform. But as can be seen from (2.5), the pressure distribution in Jeffery-Hamel flow is tied to the velocity distribution. Any agent, therefore, which makes the velocity distribution more uniform does likewise to the pressure.

Thus when $R = R_z$ and λ is large, the pressure gradient across the channel will be near zero and almost uniform. The result is a flow which resembles a near solid mass oozing very slowly through the channel. The volumetric flux, when compared with the corresponding no-slip flow, is very small and approaches zero as $\lambda \to +\infty$.

Conclusions

In this paper we have examined an exact solution of the Navier-Stokes equations subject to slip boundary conditions. We have found that in converging channel flows we can observe dramatic increases in the volumetric flow rates of slip flows over their no-slip counterparts. As the Reynolds number $|R|$ increases, however, the no-slip flows become more uniform with boundary layers of thickness $(-R)^{-1/2}$ along the walls. With $|R| \gg 1$, the propensity of large slip coefficients to enhance flow rates is reduced as evidenced by (3.14).

Slip flows in a diverging channel are much more intricate. There are five different regimes through which the flows progress as the Reynolds number increases. The most practical result may well be that even under the most favourable of circumstances, the presence of slip along the walls of a diverging channel increases the volumetric flow rate by only 15.7%.

References

1. S. Goldstein, *Modern developments in fluid dynamics*. Clarendon Press: Oxford (1938) 105–110.
2. L.E. Fraenkel, On the Jeffery-Hamel solutions for flow between plane walls. *Proc. Roy. Soc.* A 267 (1962) 119–138.
3. L. Rosenhead, *Laminar boundary layers*. Clarendon Press: Oxford (1963) 144–150.
4. G.K. Batchelor, *An introduction to fluid dynamics*. Cambridge University Press (1967) 294–302.
5. A. Hooper, B.R. Duffy and H.K. Moffatt, Flow of fluid of non-uniform viscosity in converging and diverging channels. *J. Fluid Mech.* **117** (1982) 283–304.
6. I.J. Sobey and P.G. Drazin, Bifurcations of two-dimensional channel flows. *J. Fluid Mech.* **171** (1986) 263–287.
7. Sir H. Lamb, *Hydrodynamics*, 6th ed. Dover Publications (1932) 602–604.
8. H.S. Tsien, Superaerodynamics – Mechanics of rarefied gases. J. Aeronaut. Sci. **13** (1946) 653–664.
9. J.A. Laurmann, Linearized slip flow past a semi-infinite flat plate. *J. Fluid Mech.* **11** (1961) 82–96.
10. A.I. Van de Vooren and A.E.P. Veldman, Incompressible viscous flow near the leading edge of a flat plate admitting slip. *J. Engineering Math.* **9** (1975) 235–249.
11. K. Tamada and H. Miura, Slip flow past a tangential flat plate at low Reynolds numbers. *J. Fluid Mech.* **85** (1978) 731–742.
12. H. Miura, Slip flow of a viscous fluid past an inclined flat plate. *J. Engineering Math.* **17** (1983) 41–53.
13. P.F. Byrd and M.D. Friedman, *Handbook of elliptic integrals for engineers and scientists*, 2nd ed. Springer-Verlag (1971) p. 10.